International Journal of Applied Pharmaceutics

ISSN- 0975-7058 Vol 16, Issue 6, 2024

Original Article

IDENTIFYING POTENTIAL hENR INHIBITORS AGAINST PROSTATE CANCER EMPLOYING *IN SILICO* DRUG REPURPOSING APPROACH

KAVANA KRISHNA NAYAK[1], SUMIT RAOSAHEB BIRANGAL[1], LALIT KUMAR[2], RUCHI VERMA[1*]

[1]Department of Pharmaceutical Chemistry, Manipal College of Pharmaceutical Sciences, Manipal Academy of Higher Education, Manipal, India. [2]Department of Pharmaceutics, National Institute of Pharmaceutical Education and Research, Hajipur, India
*Corresponding author: Ruchi Verma; *Email: ruchiverma.pharma@gmail.com

Received: 05 Jun 2024, Revised and Accepted: 19 Sep 2024

ABSTRACT

Objective: This study employed an *in silico* drug repurposing strategy to identify potential human enoyl acyl carrier protein reductase (hENR) inhibitors.

Methods: The co-crystallized ligand triclosan was used as a reference standard. Initially, FDA-approved drugs from the Drug Bank database were docked against the hENR and compounds with appreciable binding affinities with the protein were shortlisted. The binding energy calculations, ADME analysis, and induced-fit docking results of shortlisted compounds led to the identification of two top hits, DB07676 and DB11399, which were further subjected to molecular dynamics simulation.

Results: Of 2,509 ligands docked via High Throughput Virtual Screening (HTVS), the top 250 were assessed with Standard Precision (SP) and the top 25 with Extra Precision (XP) mode. Thirteen compounds were selected based on interactions and XP scores, ranging from-15.245 to-10.031. Relative binding free energies of ligands DB07676 and DB11399 were-54.18 and-61.38 kcalmol^{-1}, respectively. ADME analysis confirmed that both ligands followed Lipinski's Rule, though DB11399 had a high log P, which could be addressed by adding polar groups. Induced Fit scores for DB07676 and DB11399 were-10.592 and-11.220, respectively. Molecular Dynamics simulations confirmed superior stability of these complexes with RMSD ranging from 1.2 to 3.5 Å for the protein and 1.7 to 5.2 Å for the ligand with DB07676-protein complex and 1.4 to 3.0 Å for the protein and 1.1 to 5.8 Å for the ligand with DB11399-protein complex.

Conclusion: Our final findings suggested that DB07676 and DB11399 could be potential lead compounds as hENR inhibitors.

Keywords: Prostate cancer, hENR, Docking, In silico, Molecular dynamics simulation, Drug repurposing

DOI: https://dx.doi.org/10.22159/ijap.2024v16i6.51700 Journal homepage: https://innovareacademics.in/journals/index.php/ijap

INTRODUCTION

Despite advancements in cancer research, the incidence of prostate cancer in most countries has been showing an upward trend [1]. Currently, prostate cancer ranks as the second most prevalent cancer among men globally in terms of incidence rate, which can go as high as 83.4 per 100,000 people [2, 3]. Conventional cancer therapy using classical cytotoxic drugs causes indiscriminate destruction of normal cells, making them one of the most toxic drugs employed in treatment [4]. Thus, the advent of targeted therapy has tremendously revolutionized cancer research. Targeted therapy targets cancer-specific enzymes or pathological pathways, thereby causing selective destruction of cancerous cells. Thus, there is a need to develop new drugs against cancer that specifically target tumour cells with no or minimal effects on normal cells [5-7].

Reprogramming of numerous metabolic pathways has been reported in cancer cells to support their uncensored growth and proliferation [8]. One such metabolic shift that has garnered colossal attention is lipid metabolism. Lipid metabolism is an umbrella term for lipid biosynthesis, uptake, storage, mobilisation and catabolism [9]. Unlike normal cells, prostate cancer cells prefer to utilize fatty acids over glucose as their energy substrates [10]. In most cancer settings, a remarkably augmented fatty acid synthesis and the expression of an associated enzyme have been observed. Therefore, knocking down the lipogenic axis serves as a targeted approach against many types of cancers [9]. Type I Fatty Acid Synthase (FAS) is a large multidomain enzyme synthesizing long-chain saturated fatty acids. Since normal cells obtain fatty acids exogenously from the diet, FAS is scantily expressed. However, prostate cancer cells primarily rely on this enzyme for fatty acids and thus demonstrate a dramatic FAS over-expression.

Interestingly, despite high levels of circulating fatty acids, tumour cells become FAS-dependent to maintain their growth rates. Recent studies confirmed FAS to be an oncogene, and its inhibition results in selective cytotoxicity towards cancer cells [11]. FAS contains seven catalytic domains such as enoyl-acyl carrier protein-reductase, β-ketoacyl reductase, dehydratase, thioesterase, β-ketoacyl synthase, acyl carrier protein and malonyl acetyltransferase domains. Inhibition of FAS through human enoyl-Acyl Carrier Protein-Reductase (hENR) has been linked with the induction of selective apoptosis and reversal of drug resistance in tumour cells, both *in vivo* and *in vitro* [12, 13]. This vulnerable dependency of cancer cells on FAS can be exploited to develop therapeutic approaches that cause selective cytotoxicity and reverse chemotherapy resistance in prostate cancer cells without affecting normal cells. hENR is composed of four chains, namely chains A, B, C and D. These chains form a dimer of dimer wherein chains A and B dimerise to give one biological homodimer (AB dimer) and chains C and D forms CD dimer. Triclosan (TCL) binds at the hENR dimer interface instead of the active site, which inturn causes structural changes along the NADPH binding site. Thus, it behaves as an allosteric Protein-Protein Interface (PPI) inhibitor. Hence, the allosteric site is the relevant physiological binding site. The hENR domain, consisting of 1529–1867 residues, is divided into two subdomainsi. e, NADPH binding domain and substrate binding domain. The NADPH binding domain includes amino acid residues between 1651–1794, whereas the substrate binding domain contains residues between 1530–1650 and 1795–1858 [14]. The NADPH binding domain adopts a classical Rossmann fold, featuring a five-strand parallel β-sheet (β8–β12) surrounded by several helices. The reported hENR-TCL structure has two TCL binding sites, one at the AB dimer interface and another at the CD dimer interface. TCL binds against the extended β-sheet of the dimer's Rossmann fold [13].

The existing literature and clinical data underscore the absence of FDA-approved drugs for hENR domain. Several FAS inhibitors undergoing clinical trials exhibit pharmacological limitations like weight loss, neutropenia etc. Therefore, this study aims to identify potential hENR inhibitors using in silico tools. We used a drug repurposing approach as a design strategy to achieve this. Drug

repurposing involves the identification of new indications for approved or investigational drugs [15]. This approach is found to be an attractive strategy. This approach overcomes challenges like high attrition rates, significant expenses, and the laborious procedures typically associated traditional drug discovery and development [16]. Herea library of FDA-approved small molecules from the DrugBank database were screened, using a receptor-based virtual screening approach. The prepared ligands were docked against the crystal structure of hENR (PDB 4W9N) obtained from the protein data bank. Molecules based on docking scores and interactions were further subjected to MMGBSA, ADME, and induced fit docking. The top identified ligands were subjected to molecular dynamics simulations for studying the interactions with amino acid residues and stability of the hENR-ligand complex. TCL, a known hENR inhibitor, was employed as the reference standard and subjected to all the *in silico* investigations performed on ligands [13, 17, 18]. The results of the ligands were then compared with those of the standard. All the computational analyses were performed using Schrodinger 12.7. This study identifies two promising scaffolds that could potentially be developed into novel and potent hENR inhibitors against prostate cancer.

MATERIALS AND METHODS

Computational simulations software used

All the in silico investigations were performed on the Schrödinger Suite (version 12.7) Maestro graphical user interface (www.schrodinger.com) on an HP computer with a Linux Ubuntu 18.04.1 lts as operating system, Intel Haswell graphics card, 4GB RAM and Intel Core i3 processor.

Protein selection for docking

The link between prostate cancer development and FAS over-expression is well established [10, 12]. Since FAS knockdown through the hENR domain causes selective cytotoxicity, hENR acts as a promising target to destroy cancer cells by depriving them of vital fatty acids to keep up their growth rates [19]. This study used the crystal structure of hENR complexed with triclosan, PDB 4W9N (1.84 Å resolution) from Protein Data Bank (RSCB PDB).

Protein preparation for docking

Utilizing the Protein Preparation Wizard panel of the Maestro interface, the retrieved protein was produced at a pH of 7 using – import and process, review and modify, and refine functions of Maestro sequentially. In the import and process tab, bond orders were assigned using the Chemical Component Dictionary (CCD) database, hydrogens were added, and zero-order bonds were created for metals and disulfide bonds. In the refine tab, sample water orientation was chosen using PROPKA at a pH of 7 for the H-bond assignment. The gaps in the side chains and loops were filled utilizing the Prime module, and waters beyond 5 Å were deleted. The protein structure was then energy minimized using the force field of OPLS4. A grid was generated using a receptor Grid Generation tool of Maestro. The binding pocket of the protein into which the ligands bind was identified using the Site Map tool. hENR is composed of four chains, namely chains A, B, C and D. This enzyme is a dimer of dimer, wherein chains A and B form AB homodimer and chains C and D form CD homodimer. These two homodimers (AB homodimer and CD homodimer) come together to form hENR. This enzyme houses two binding sites, one at the AB dimer interface and another at the CD dimer interface (fig. 1a and fig. 1b). Ligands binding at the AB interface binding site interacts with amino acid residues of chains A and B. Similarly, ligands binding to the CD interface binding site engage with amino acid residues of chains C and D [13]. Since dimers AB and CD are identical, for the sake of simplicity, we worked with only chains A and B (fig. 2). Chains C and D of hENR were excluded because working with all chains would be unnecessary and cumbersome.

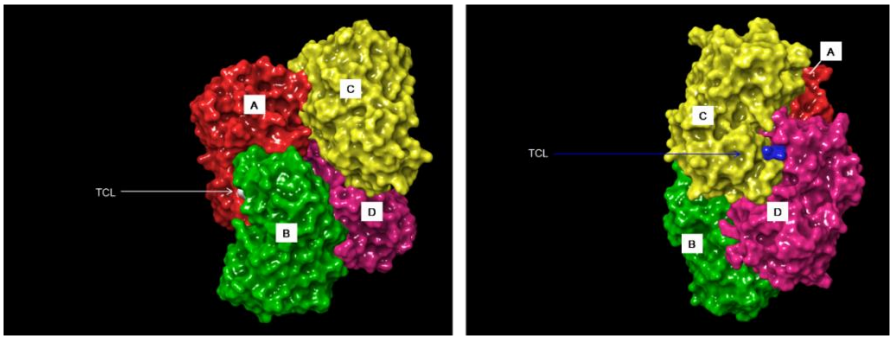

Fig. 1: 3D diagrammatic representation of four chains and two TCL-binding sites of hENR) TCL (in white) at the AB dimer interface, b) TCL (in blue) at the CD dimer interface

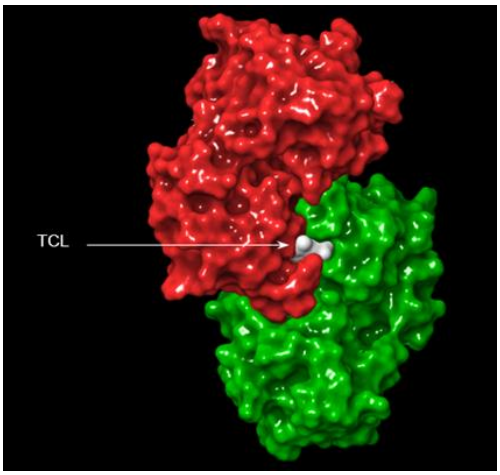

Fig. 2: 3D diagrammatic representation of the hENR chain A and B

Ligand preparation for docking

Following protein preparation, ligand preparation was performed using the Epik tool of the Maestro LigPrep panel at a pH of 7, keeping the parameters as default. Ionization was set to Generate possible states at pH 7.0+/-2.0. Subsequently, all the ligands were desalted, and their tautomers were generated. Computations were carried out by retaining specified chiralities. The prepared 3D structures of ligands were then energy minimized [20, 21].

Ligand docking

The prepared ligands were docked to the protein using the Grid-based Ligand Docking with Energetics (GLIDE) tool [20, 21]. This tool provides valuable insights into the binding affinities between the ligand and the receptor, allowing for an in-depth exploration of their interaction. Based on the procured data, the tool further allots a docking score for each ligand and ranks them in the descending order of their scores. Moreover, this tool provides different options based on speed versus accuracy, namely High-Throughput Virtual Screening (HTVS), Standard Precision (SP) and Extra Precision (XP). HTVS mode docks faster with lower accuracy, whereas XP mode is the most accurate and consumes more time. Thus, HTVS, SP and XP serve as hierarchical filters in screening molecules and identifying those with appreciable binding capabilities. At first, all the prepared ligands were screened through HTVS and the best-identified ligands were further subjected to screening by SP and XP modes sequentially [22-24].

Binding energy calculation

The time span for which the interaction between ligand and protein persists depends on the binding energy of the interaction, which is estimated by the Prime module using the MM-GBSA (Molecular Mechanics, the Generalized Born model and Solvent Accessibility) approach [25]. This method is based on the model of Variable-dielectric generalized Bron (VSGB) salvation, which employs water as a solvent under the OPLS3e force field [22, 23]. Based on their dock score from XP docking, the top thirteen ligands were identified and subjected to MM/GBSA analysis.

ADME analysis

The ADME analysis was carried out using Maestro's QikProp tool to estimate a ligand's druggability [13, 26]. The QikProp tool measures parameters such as molecular weight (MW), octanol/water partition coefficient (QPlogPo/w), number of hydrogen bond donors (donorHB) and hydrogen bond acceptors (accept HB) of the ligands [27-29].

Induced fit docking

Thirteen ligands were shortlisted based on their XP docking score, binding energy calculation and ADME analysis for Induced Fit Docking (IFD). IFD protocol generates multiple ligand binding poses and the corresponding structural changes at the binding site, which allows the ligand to bind better. This is performed using Glide and Prime modules. The standard protocol generates 20 poses per ligand was utilized, and Van der Waals scaling was performed at a default factor of 0.50 [30, 25]. An IFD score was generated based on the docking score, glide energy, glide emodel values, and types of interactions [26].

Molecular dynamics

Desmond module of Schrodinger was used for MD studies. Dock complexes of the top two ligands and TCL (reference compound) were exposed to MD simulation studies. Molecular dynamics involved the following steps: firstly, the protein-ligand complex was chosen, an orthorhombic simulation box of 10Å was generated, and system neutralization was done by adding Na+ions using System Builder [31]. Further, the system was energy minimized and maintained at a temperature of 300 K and a pressure of 1.01325 bars, wherein the method of Nose-Hoover and method of Martina-Tobias-Klein were employed as thermostat and barostat, respectively [23, 24]. Collectively, 1000 frames were recorded in a period of 100-nsec simulation. MD results were analyzed with the help of simulation interaction diagrams [32, 33].

RESULTS AND DISCUSSION

Molecular docking

Docking was performed using various modes of the GLIDE panel. The prepared 2,509 ligands were subjected to docking in HTVS mode. HTVS mode is employed to screen many compounds as it consumes less time as compared to SP and XP modes. In HTVS docking, conformational sampling is more constrained than SP docking and cannot be employed with score-in-place. Resulting best 10% of resulting ligands from HTVS are identified based on their docking score and are further subjected to SP docking, which summed up to 250 compounds. Docking in SP mode retains a fine balance between speed and accuracy. The top 10% of resulting ligands from SP mode are subjected to XP docking, which summed up to 25 ligands. XP docking employs descriptors and explicit water technology. This mode filters out false-positive results and thus ensures a reliable correlation between the docking score and the binding pose of ligands [23]. Lastly, the top thirteen compounds were selected based on their XP docking score and protein-ligand interactions. The docking score of all these ligands ranged from-15.245 to-10.031kcalmol-1. TCL in the AB dimer interface engages with hydrophobic side chain residues of both chains A and B through van der Waals interactions. Key amino acid residues of chain A include LEU1753, LEU1780, ILE1784, and PHE1791, and those of chain B include LEU1753, LEU1780, and PHE1791 [14]. All the ligand-protein interactions, such as H-bond, hydrophobic interactions, π-cation, charged positive and negative interactions formed by the top thirteen ligands, are summarized in table 1.

Among thirteen ligands and TCL, DB08909, DB03115, DB07676, DB11519, DB07101, and DB09289 formed an H-bond with LEU1780. The only ligand that formed aromatic π-cation stacking with PHE1791 was DB09289. Aromatic π-π stacking was observed with DB11855, DB07783, DB03115, DB07676, DB11519, DB11399, DB07101, DB08984, DB12390 and DB09289 with PHE1791. The cocrystal engaged with PHE1791 through aromatic π-π stacking through rings A and B.

MM-GBSA

Selected top thirteen ligands were subjected to Prime MM-GBSA analysis in the chosen docked poses to estimate stability of protein-ligand complexes as a measure of binding energy. The relative binding free energy (dG) of all the protein-ligand complexes was determined to be less than-14kcalmol^{-1} (table 2). dG of the co-crystallized ligand was determined to be-31.1 kcalmol^{-1}. Thus, the results of this analysis show that all the ligands possess stability in their docked poses and, therefore, can act as potential hENR inhibitors. Of the thirteen ligands, DB08909 exhibited the most favourabledG of-67.07kcalmol^{-1}.

ADME

The top 13 compounds were analysed for their ADME properties using the QikProp tool. These properties included molecular weight, number of hydrogen bond donors, number of H-bond acceptors, predicted octanol/water partition coefficient (Log Po/w), predicted IC50 value (QPlog HERG), predicted aqueous solubility (QPLog S), predicted blood/brain partition coefficient (Log BB), polar surface area (PSA) and Lipinski rule of five (table 3). Lipinski's rule of five employs molecular descriptors such as molecular weight, hydrogen bond donors, hydrogen bond acceptors and octanol-water partition coefficient (log P). The rule states that molecules with molecular weight<500 Da, hydrogen bond donors ≤5, hydrogen bond acceptors ≤10 and logP ≤ 5 are considered "drug-like". An orally active compound is considered drug-like only if there is not more than one violation of the given criteria [24]. The eleven ligands out of thirteen that obeyed the rule of five were DB11855, DB00938, DB12100, DB07783, DB03115, DB07676, DB11519, DB07101, DB08984, DB12390, DB09289. The high logP value of DB11399 could be reduced by incorporating polar groups. The co-crystallized ligand, TCL, was also in accordance with the rule.

Table 1: 2D interaction diagrams of top thirteen ligands from XP

S. No.	Drug	2D interaction diagram	Interacting residues
1	DB11855	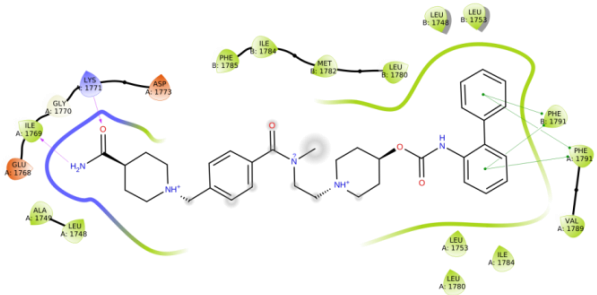	**Hbond:** A: LYS 1771, A: ILE 1769 **π-π stacking:** A: PHE 1791, B: PHE 1791 **Charged Positive:** A: LYS 1771
2	DB00938	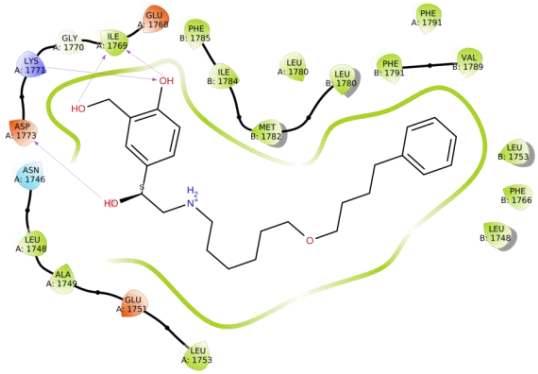	**H bond:** A: ILE 1769, A: LYS 1771, A: ASP 1773 **Charged Positive:** A: LYS 1771 **Charged Negative:** A: ASP 1773
3	DB08909	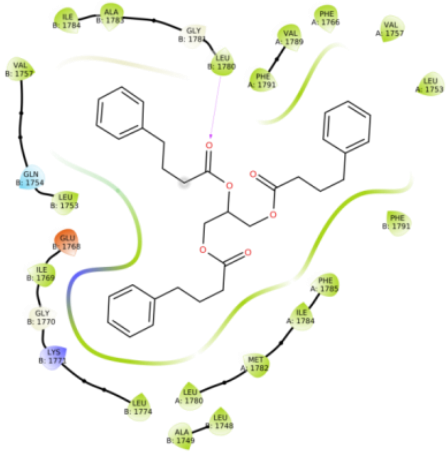	**H bond:** B: LEU 1780
4	DB12100	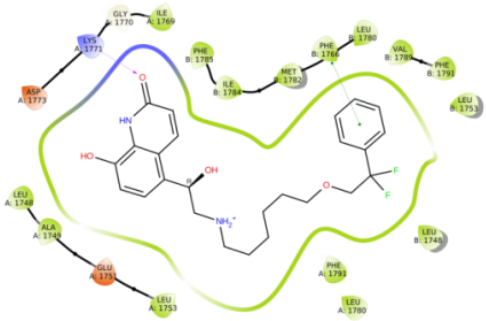	**H bond:** A: LYS 1771 **π-π stacking:** B: PHE 1766 **Charged Positive:** A: LYS 1771
5	DB07783	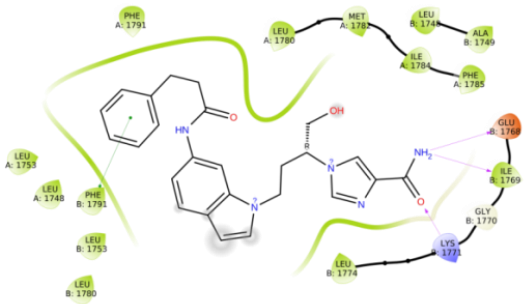	**H bond:** B: GLU 1768, B: ILE 1769, B: LYS 1771 **π-π stacking:** B: PHE 1791 **Charged Positive:** B: LYS 1771

S. No.	Drug	2D interaction diagram	Interacting residues
6	DB03115	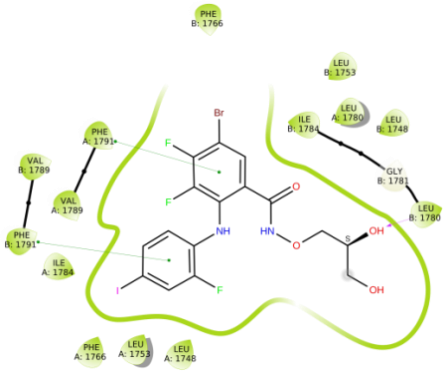	**H bond:** B: LEU 1780 **π-π stacking:** A: PHE 1791, B: PHE 1791
7	DB07676	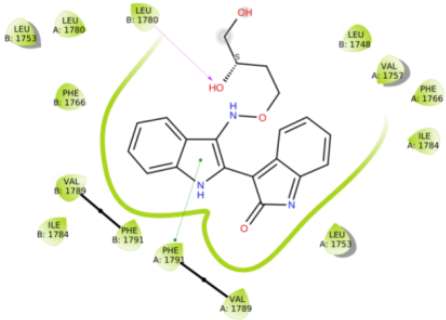	**H bond:** B: LEU 1780 **π-π stacking:** A: PHE 1791
8	DB11519	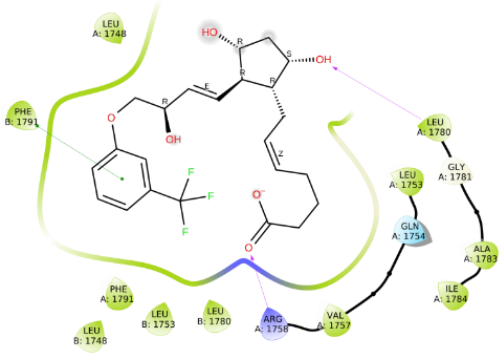	**H bond:** A: LEU 1780, A: ARG 1758 **π-π stacking:** B: PHE 1791 **Charged Positive:** A: ARG 1758
9	DB11399	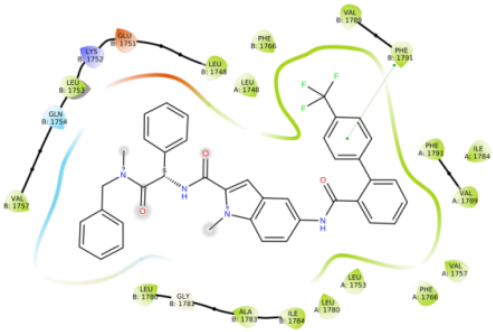	**π-π stacking:** B: PHE 1791
10	DB07101	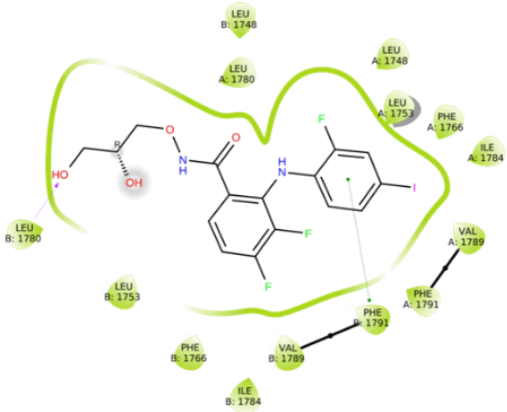	**H bond:** B: LEU 1780 **π-π stacking:** B: PHE 1791

S. No.	Drug	2D interaction diagram	Interacting residues
11	DB08984	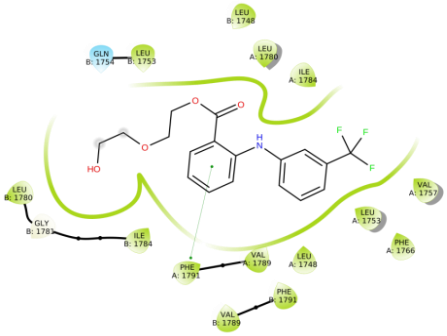	**π-π stacking:** A: PHE 1791
12	DB12390	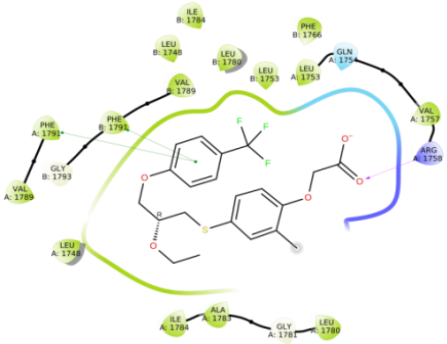	**H bond:** A: ARG 1758 **π-π stacking:** A: PHE 1791, B: PHE 1791 **Charged Positive:** A: ARG 1758
13	DB09289	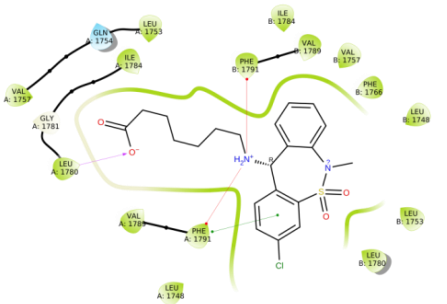	**H bond:** A: LEU 1780 **π-π stacking:** A: PHE 1791 **π-cation interaction:** A: PHE 1791, B: PHE 1791
14	TCL	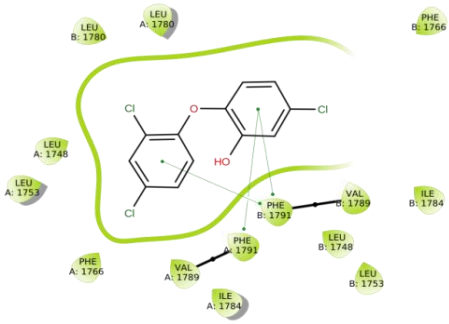	**π-π stacking:** A: PHE 1791, B: PHE 1791

Table 2: Relative binding free energy and docking score of top thirteen ligands

S. No.	Drugs	Docking score (XP)(kcal mol^{-1})	MMGBSA dGbind[a] (kcalmol^{-1})
1	DB11855	-11.465	-65.68
2	DB00938	-13.645	-65.78
3	DB08909	-14.102	-67.07
4	DB12100	-15.245	-45.08
5	DB07783	-12.195	-40.40
6	DB03115	-13.422	-52.59
7	DB07676	-11.23	-54.18
8	DB11519	-13.462	-37.74
9	DB11399	-11.220	-61.38
10	DB07101	-12.118	-51.90
11	DB08984	-13.245	-37.52
12	DB12390	-11.575	-44.02
13	DB09289	-10.031	-14.13
14	TCL	-6.332	-31.1

[a]Relative binding free energy

Table 3: ADME analysis of the top thirteen ligands using Qikproptool

Compounds	MW[a]	Donor HB[b]	AccptHB[c]	QPlogP$_{o/w}$[d]	QPlogHERG[e]	QPlogS[f]	QPlogBB[g]	PSA[h]	Rule of five[i]
DB11855	597.756	3	12	3.552	-7.759	-4.508	-1.394	133.115	1
DB00938	415.572	4	7.35	3.939	-7.673	-4.302	-1.782	81.662	0
DB08909	530.66	0	6	8.103	-8.821	-9.579	-2.341	106.336	2
DB12100	460.52	4	8.15	3.332	-7.826	-4.704	-2.124	101.349	0
DB07783	445.52	4	8.75	3.158	-7.473	-5.856	-2.722	128.354	0
DB03115	561.093	3	7.1	3.443	-5.777	-5.76	-1.123	103.177	1
DB07676	335.388	3	8.6	1.75	-5.905	-3.545	-1.67	121.174	0
DB11519	458.474	4	7.85	4.118	-3.905	-5.428	-2.165	115.657	0
DB11399	674.721	1.25	7.25	8.103	-7.597	-10.267	-0.943	92.27	2
DB07101	482.197	3	7.1	3.016	-5.9	-5.098	-1.173	101.153	0
DB08984	369.34	1	4.9	4.505	-6.249	-5.833	-0.792	76.145	0
DB12390	444.465	1	5.7	5.864	-4.395	-6.814	-0.958	71.961	1
DB09289	436.952	2	8	1.118	-4.062	-4.069	-1.071	101.541	0
TCL	289.545	1	1.25	4.756	-4.887	-4.516	0.459	28.291	0

[a]Molecular weight (range 130.0 –725.0), [b]Estimated number of hydrogen bonds that would be donated by the solute to water molecules in an aqueous solution (range 0.0–6.0), [c]Estimated number of hydrogen bonds that would be accepted by the solute from water molecules in an aqueous solution (range 2.0–20.0), [d]Predicted octanol/water partition coefficient (range –2.0 to 6.5), [e]Predicted IC50 value for blockage of HERG K+channels(concern below –5), [f]Predicted aqueous solubility (range –6.5 – 0.50), [g]Predicted brain/blood partition coefficient (range −3.0 to 1.2), [h]PSA Van der Waals surface area of polar nitrogen and oxygen atoms (range 7.0–200.0), [i]Number of violations of Lipinski's rule of five. The rules are: MW<500, QPlogPo/w<5, donor HB ≤ 5, acceptHB ≤ 10 (range ≥ 4)

Induced fit docking

In standard virtual docking, ligands are docked against the receptor's binding site; the receptor is often assumed to be rigid. Whereas most receptor-binding sites undergo conformational changes in their shape and binding mode during the binding process. These changes enable the receptor and ligand to better interact with each other. This is known as induced fit [29]. Thus, induced fit docking is done to take into consideration the flexibility of the receptor binding site and provide accurate and reliable insights into the binding affinity of the ligands. IFD protocol filters out false negatives, employing additional confirmations rather than docking against a single conformation of a receptor. Among the best thirteen ligands, DB12100 exhibited the most favourable dock score of-15.245. 3D receptor-ligand interactions of the best two ligands are shown in (fig. 3).

A comparison of new and missing interactions during IFD to XP is shown in (table 4).

Table 4: New and missing interactions of top compounds from IFD versus XP and their IFD scores

S. No.	Ligands	H-bond[a]		π-π stacking		Salt bridge		IFD Score[b] (kcal mol^{-1})
		New	Missing	New	Missing	New	Missing	
1	DB11855	A: LEU1780 A: ASP1773	A: LYS1771	-	-	A: ASP1773 A: GLU1751	-	-11.465
2	DB00938	-	-	-	-	A: GLU1751	-	-13.645
3	DB08909	A: LEU 1780	-	-	-	-	-	-14.102
4	DB12100	B: GLU1751 B: ILE1769 B: LYS1771	A: LYS1771	-	-	B: GLU1751	B: PHE1766	-15.245
5	DB07783	B: GLY1754	B: GLU1768 B: ILE1769 B: LYS1771	A: PHE1791	B: PHE1791	-	-	-12.195
6	DB03115	B: LEU1767 B: SER1747	B: LEU1780	-	B: PHE1791	-	-	-13.422
7	DB07676	A: GLY1781 A: LEU1780 A: LEU1753	B: LEU1780	B: PHE 1791	A: PHE1791	-	-	-10.592
8	DB11519	B: ARG1758 B: LEU1780	A: LEU1780 A: ARG1758	-	B: PHE1791	-	-	-13.390
9	DB11399	A: LEU1780 B: LEU1780	-	A: PHE1766 A: PHE1791	-		-	-11.220
10	DB07101	-	B: LEU1780	A: PHE1791	B: PHE1791	-	-	-12.118
11	DB08984	B: SER1747 B: LEU1767	-	-	A: PHE1791	-	-	-12.956
12	DB12390	-	A: ARG1758	-	A: PHE1791	B: ARG1758	-	-11.379
13	DB09289	A: PHE1766 A: GLY1781	-	-	-	-	-	-10.031

[a]hydrogen bond, [b]Induced Fit Docking Score

Molecular dynamics

Amongst all ligands under investigation, DB07676 and DB11399 were further taken up for MD studies based on XP docking score, binding interactions with protein, ADME parameters and IFD score. These ligands, in their best binding pose from IFD, were used. RMSD fluctuations of ligand-protein complexes, namely, DB07676-hENRdocked complex (complex 1), DB11399–hENR docked complex (complex 2), and TCL– protein complex (complex 3), were measured individually. In Complex 1, the RMSD values of protein and ligand

were within the range of 1.2 to 3.5 Å and 1.7 to 5.2 Å, respectively. Major drifts were observed during 5-36 ns and 82-100 ns. However, during this period, the RMSD values were within the acceptable range of 1-3 Å (fig. 4a). In complex 2, the protein and ligand RMSD values were determined to be within the range of 1.4 to 3.0 Å and 1.1 to 5.8 Å, respectively. The complex was found to be stable throughout the study, but slight drifts were observed during 8-25 ns and 54-88 ns (fig. 4b). For the co-crystallized ligand-hENR complex, the RMSD values of protein and ligand were within the range of 1.25 to 3.875Å and 0.5-6.5 Å, respectively. Major drift was observed during 17-83 ns, after which the complex stabilized towards the end of the study (fig. 4c).

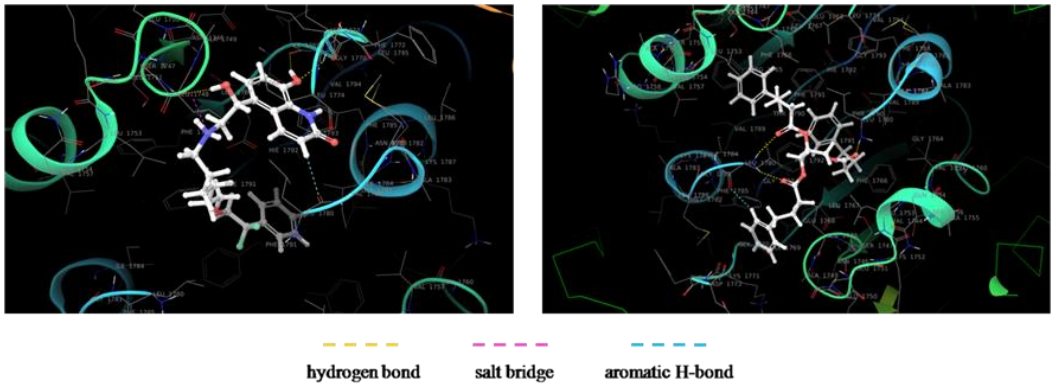

Fig. 3: 3D ligand interactions from IFD of a) DB12100, b) DB08909 with hENR

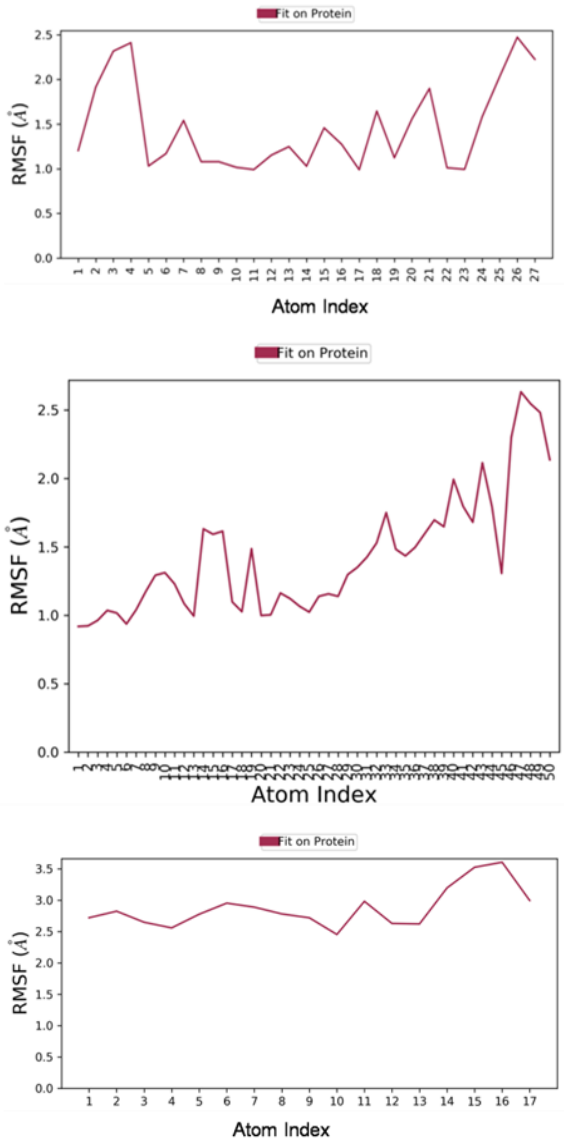

Fig. 4: RMSD plot of a) DB07676-hENR complex, b) DB11399-hENR complex, c) TCL-hENR complex

Protein-ligand interactions were observed throughout the MD simulations, and an analysis report for the potential interactions was produced. In the selected trajectory, protein-ligand interactions occurring for more than 30.0 percent of the simulation time were recorded. In complex 1, the ligand DB07676 formed water-bridged interactions with GLU1768 of chain B through the ligand's nitrogen-atom of indole moiety. Hydrophobic interactions and hydrogen bonds were also present but with weaker occupancy. Hydrophobic interactions were seen with LEU1780, ILE1784 PHE1791 of chain A, and LEU1753, VAL1757, PHE1766, and PHE1791 of chain B. The ligand formed hydrogen bonds with GLN1754, LEU1780, and GLY1781 of chain A and LEU1780 of chain B (fig. 5a). In complex 2, the ligand DB11399 showed π-π stacking interaction with PHE 1766 residue of chain B. The ligand also interacted with LEU 1753 of chain B through water-bridged interactions. Hydrogen bonds and other hydrophobic interactions were also present but with weaker occupancy. Hydrogen bonds were seen with GLY1754 and GLY1781 of chain A and GLN1754 AND LEU1780 of chain B. Hydrophobic interactions were seen with LUE1753, VAL1757, PHE1766, ILE17891, and PHE1791 of chain A; and LEU1748, LEU1753, LEU1780, ILE1784 and PHE 1791 of chain B (fig. 5b). Co-crystallized ligand-hENR complex formed π-π stacking interaction with PHE1791 of chain B through its ring A. Hydrogen bonds with weaker occupancy were observed with LEU1780 of chain A, and GLU1768, LEU1780 of chain B (fig. 5c).

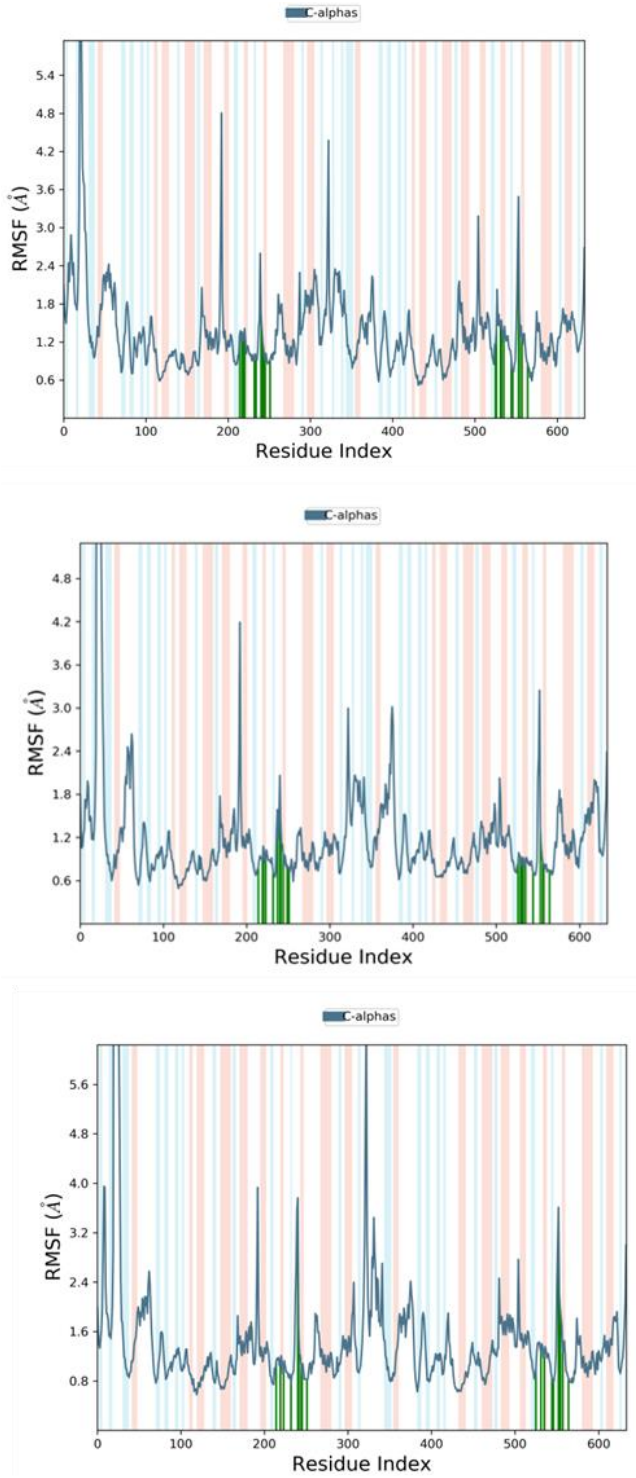

Fig. 5: Protein-ligand interaction diagram of a) DB07676-hENR, b) DB11399 hENR, c) TCL (co-crystallized ligand)-hENR complex

P-RMSF (Protein Root mean Square Fluctuations) was performed to visualize fluctuations of segments along the protein during the simulation study. The amino acid residue of the protein undergoing more fluctuations is represented by higher peaks.

For complex 1, the residue in the binding site that showed the highest fluctuation was B: LEU1780 with an RMSF value of 3.49Å, A: ASP1773 with an RMSF value of 2.60Å and B: ASP1773 with RMSF value of 1.86Å. RMSF values of the remaining protein were in the range of 0.52Å to 8.17Å (fig. 6a). For complex 2, the most fluctuating binding site residues were B: LEU1774 with an RMSF value of 3.24Å, B: ASP1773 with an RMSF value of 2.32Å and A: LEU1780 with an RMSF value of 2.06Å. RMSF values of the remaining protein ranged between 0.54Å to 8.76Å (fig. 6b). For complex 3, the most volatile residues in the binding site were A: LEU1780 with an RMSF value of 3.76Å, B: LEU1774 with an RMSF value of 3.61Å and A: ASP1773 with an RMSF value of 3.58Å. The RMSF values of the remaining protein ranged between 0.58Å to 12.99 Å (fig. 6c).

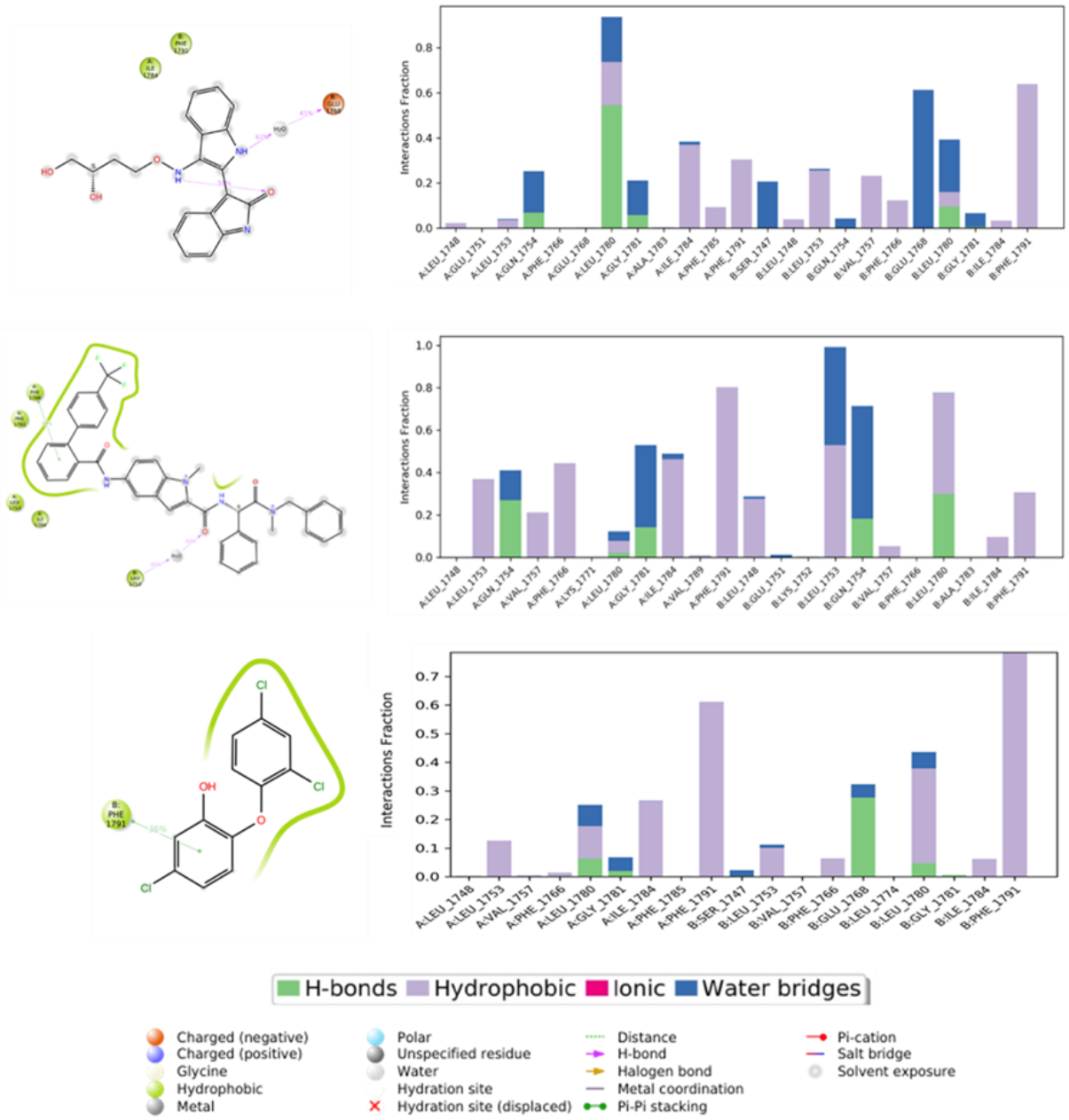

Fig. 6: Protein RMSF plot of a) DB07676, b) DB11399 c) TCL during MD simulations

Ligand Root Mean Square Fluctuation (L-RMSF) provides insights into the interaction of ligand fragments with proteins, throwing light on their binding dynamics and entropic contributions involved during the process of binding. For complex 1, the RMSF value of major volatility was observed with C2 alkene at position 26 with an RMSF value of 2.47 Å. Other fluctuations were observed with the O3 group at the 4th position and the O2 group at the 3rd position with an RMSF value of 2.41Å and 2.32Å, respectively (fig. 7a). For complex 2, major volatility was seen with C2 alkene at position 47 with an RMSF value of 2.63Å. Other fluctuations observed with the ligand were C2 at positions 49 and 46 with an RMSF value of 2.48Å and 2.30Å, respectively (fig. 7b). For complex 3, the RMSF value of major volatility was observed in the chlorine atom at 16th position 47 with an RMSF value of 3.61Å. Other fluctuations observed with the ligand were chlorine atoms at the 15th and 14th position with an RMSF value of 3.53Å and 3.20Å, respectively (fig. 7c).

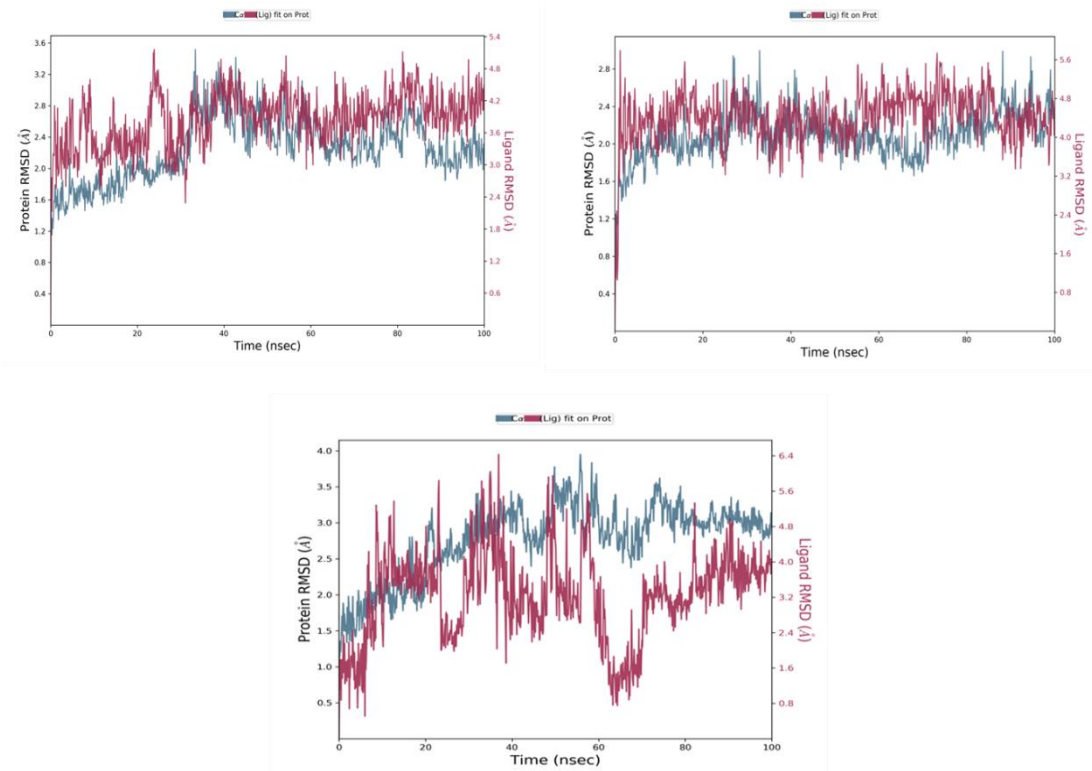

Fig. 7: Ligand RMSF plot of a) DB07676, b) DB11399, c) TCL (cocrystallised ligand) during MD simulations

CONCLUSION

In this research study, receptor-based virtual screening was performed on the target enzyme (4W9N) to identify potential hENR inhibitors. FDA-approved drugs from the Drug Bank database were prepared and docked against the binding site of hENR. Top molecules were identified, assessed and ranked based on their docking score, binding energy, fitness score, ADME parameters and results of MD study. Our final findings suggested that DB07676 and DB11399 can behave as potential leads against prostate cancer as hENR inhibitors. However, *in vitro* and *in vivo* studies need to substantiate these findings further for their selective cytotoxicity to facilitate the repurposing of these molecules in prostate cancer.

ACKNOWLEDGEMENT

The authors acknowledge Manipal Schrodinger Centre for Molecular Simulations, Manipal College of Pharmaceutical Sciences and Vision Group on Science and Technology (VGST), Karnataka (KSTePS/VGST-RGS/F/GRD No.709/2017-18) for supporting and furnishing the facilities required for the smooth and effective conduct of this work.

FUNDING

The authors declare that they have no known competing financial interests or personal relationships that could have appeared to influence the work reported in this paper.

AUTHORS CONTRIBUTIONS

Kavana Krishna Nayak was involved in writing the manuscript, conducting the literature search, collecting data, and providing resources. Sumit Raosaheb Birangal contributed through supervision, design, and providing resources. Lalit Kumar played a role in the critical review, literature search, supervision, and design. Ruchi Verma was involved in conceptualization, critical review, literature search, interpretation, design, providing resources, and writing the manuscript.

CONFLICT OF INTERESTS

Declared none

REFERENCES

1. Mouchati C, Abdallah N, Jani C, Mariano M, Jani RT, Marshall DC. Trends in disease burden from prostate cancer amongst different regions of the world and extensively the European Union 15+ countries from 1990 to 2019: estimates from the global burden of disease study. J Clin Oncol. 2022;40 Suppl 6:187. doi: 10.1200/JCO.2022.40.6_suppl.187.
2. Sung H, Ferlay J, Siegel RL, Laversanne M, Soerjomataram I, Jemal A. Global cancer statistics 2020: GLOBOCAN estimates of incidence and mortality worldwide for 36 cancers in 185 countries. CA Cancer J Clin. 2021 May;71(3):209-49. doi: 10.3322/caac.21660, PMID 33538338.
3. Giona S. The epidemiology of prostate cancer Bott SR Ng KL, editors. Brisbane: Exon Publications; 2021. p. 1-17.
4. Perez Herrero E, Fernandez Medarde A. Advanced targeted therapies in cancer: drug nanocarriers the future of chemotherapy. Eur J Pharm Biopharm. 2015;93:52-79. doi: 10.1016/j.ejpb.2015.03.018, PMID 25813885.
5. Nawaz K, Webster RM. The non-small cell lung cancer drug market. Nat Rev Drug Discov. 2016;15(4):229-30. doi: 10.1038/nrd.2016.42, PMID 27032828.
6. Ali R, Mirza Z, Ashraf GM, Kamal MA, Ansari SA, Damanhouri GA. New anticancer agents: recent developments in tumor therapy. Anticancer Res. 2012;32(7):2999-3005. PMID 22753764.
7. Lee YT, Tan YJ, Oon CE. Molecular targeted therapy: treating cancer with specificity. Eur J Pharmacol. 2018 Sep 5;834:188-96. doi: 10.1016/j.ejphar.2018.07.034, PMID 30031797.
8. Fadaka A, Ajiboye B, Ojo O, Adewale O, Olayide I, Emuowhochere R. Biology of glucose metabolization in cancer cells. J Oncol Sci. 2017;3(2):45-51. doi: 10.1016/j.jons.2017.06.002.
9. Chen Y, LI P. Fatty acid metabolism and cancer development. Science Bulletin. 2016;61(19):1473-9. doi: 10.1007/s11434-016-1129-4.
10. Galbraith L, Leung HY, Ahmad I. Lipid pathway deregulation in advanced prostate cancer. Pharmacol Res. 2018;131:177-84. doi: 10.1016/j.phrs.2018.02.022, PMID 29466694.
11. Liu H, Liu JY, WU X, Zhang JT. Biochemistry molecular biology and pharmacology of fatty acid synthase an emerging therapeutic target and diagnosis/prognosis marker. Int J Biochem Mol Biol. 2010;1(1):69-89. PMID 20706604.

12. DE Piano M, Manuelli V, Zadra G, Loda M, Muir G, Chandra A. Exploring a role for fatty acid synthase in prostate cancer cell migration. Small GTPases. 2021;12(4):265-72. doi: 10.1080/21541248.2020.1826781, PMID 33043786.
13. Sippel KH, Vyas NK, Zhang W, Sankaran B, Quiocho FA. Crystal structure of the human fatty acid synthase enoyl acyl carrier protein reductase domain complexed with triclosan reveals allosteric protein-protein interface inhibition. J Biol Chem. 2014;289(48):33287-95. doi: 10.1074/jbc.M114.608547, PMID 25301948, PMCID PMC4246086.
14. Maier T, Leibundgut M, Ban N. The crystal structure of a mammalian fatty acid synthase. Science. 2008;321(5894):1315-22. doi: 10.1126/science.1161269, PMID 18772430.
15. Zhang X, Che C. Drug repurposing for parkinsons disease by integrating knowledge graph completion model and knowledge fusion of medical literature. Future Internet. 2021;13(1):14. doi: 10.3390/fi13010014.
16. Pushpakom S, Iorio F, Eyers PA, Escott KJ, Hopper S, Wells A. Drug repurposing: progress challenges and recommendations. Nat Rev Drug Discov. 2019;18(1):41-58. doi: 10.1038/nrd.2018.168, PMID 30310233.
17. Honkisz E, Zieba Przybylska D, Wojtowicz AK. The effect of triclosan on hormone secretion and viability of human choriocarcinoma JEG-3 cells. Reprod Toxicol. 2012;34(3):385-92. doi: 10.1016/j.reprotox.2012.05.094, PMID 22677473.
18. Deepa PR, Vandhana S, Jayanthi U, Krishnakumar S. Therapeutic and toxicologic evaluation of anti lipogenic agents in cancer cells compared with non-neoplastic cells. Basic Clin Pharmacol Toxicol. 2012;110(6):494-503. doi: 10.1111/j.1742-7843.2011.00844.x, PMID 22151915.
19. Lupu R, Menendez JA. Pharmacological inhibitors of fatty acid synthase (FASN) catalyzed endogenous fatty acid biogenesis: a new family of anti-cancer agents. Curr Pharm Biotechnol. 2006;7(6):483-93. doi: 10.2174/138920106779116928, PMID 17168665.
20. Jays J, Saravanan J. A molecular modelling approach for structure-based virtual screening and identification of novel isoxazoles as potential antimicrobial agents against S. aureus. Int J Pharm Pharm Sci. 2024;16(4):36-41. doi: 10.22159/ijpps.2024v16i4.49731.
21. Mathew C, Lal N, Aswathy TR, Varkey J, Varkey J. Antioxidant anticancer and molecular docking studies of novel 5-benzylidene substituted rhodanine derivatives. Int J Pharm Pharm Sci. 2023;15(7):7-19. doi: 10.22159/ijpps.2023v15i7.47421.
22. Verma R, Boshoff HI, Arora K, Bairy I, Tiwari M, Varadaraj BG. Synthesis evaluation molecular docking and molecular dynamics studies of novel N-(4-[pyridin-2-yloxy]benzyl)arylamine derivatives as potential antitubercular agents. Drug Dev Res. 2020;81(3):315-28. doi: 10.1002/ddr.21623, PMID 31782209.
23. Choudhary MI, Shaikh M, Tul Wahab A, UR Rahman A. In silico identification of potential inhibitors of key SARS-CoV-2 3CL hydrolase (Mpro) via molecular docking MMGBSA predictive binding energy calculations and molecular dynamics simulation. PLOS ONE. 2020;15(7):e0235030. doi: 10.1371/journal.pone.0235030, PMID 32706783.
24. Parasuraman S, Raveendran R, Vijayakumar B, Velmurugan D, Balamurugan S. Molecular docking and ex vivo pharmacological evaluation of constituents of the leaves of Cleistanthus collinus (Roxb.) (Euphorbiaceae). Indian J Pharmacol. 2012;44(2):197-203. doi: 10.4103/0253-7613.93848, PMID 22529475.
25. Verma R, Bairy I, Tiwari M, Bhat GV, Shenoy GG. In silico studies synthesis and anticancer activity of novel diphenyl ether based pyridine derivatives. Mol Divers. 2019 Aug;23(3):541-54. doi: 10.1007/s11030-018-9889-1, PMID 30430400.
26. Mishra H, Singh N, Lahiri T, Misra K. A comparative study on the molecular descriptors for predicting drug-likeness of small molecules. Bioinformation. 2009;3(9):384-8. doi: 10.6026/97320630003384, PMID 19707563, PMCID PMC2728118.
27. Kumar S, Chowdhury S, Kumar S. In silico repurposing of antipsychotic drugs for Alzheimers disease. BMC Neurosci. 2017;18(1):76. doi: 10.1186/s12868-017-0394-8, PMID 29078760.
28. Harshitha T, Vinak KT, Vineetha T. In silico characterization molecular docking and *in vitro* evaluation of triazole derivatives as potential anticancer agents. Asian J Pharm Clin Res. 2021;14(2):22-8. doi: 10.22159/ajpcr.2021.v14i2.40053.
29. Sai GC, Jays J, Madriwala B. Design binding affinity studies and in silico ADMET predictions of novel isoxazoles as potential anti-bacterial. Int J Curr Pharm Sci. 2022;14(4):74-7. doi: 10.22159/ijcpr.2022v14i4.2001.
30. Barreca ML, Iraci N, DE Luca L, Chimirri A. Induced fit docking approach provides insight into the binding mode and mechanism of action of HIV-1 integrase inhibitors. Chem Med Chem. 2009;4(9):1446-56. doi: 10.1002/cmdc.200900166, PMID 19544345.
31. Veenstra SJ, Rueeger H, Voegtle M, Lueoend R, Holzer P, Hurth K. Discovery of amino-1,4-oxazines as potent BACE-1 inhibitors. Bioorg Med Chem Lett. 2018;28(12):2195-200. doi: 10.1016/j.bmcl.2018.05.003, PMID 29764741.
32. Chintha C, Carlesso A, Gorman AM, Samali A, Eriksson LA. Molecular modeling provides a structural basis for PERK inhibitor selectivity towards RIPK1. RSC Adv. 2019;10(1):367-75. doi: 10.1039/c9ra08047c, PMID 35558862.
33. Sachdeo R, Khanwelkar C, Shete A. In silico exploration of berberine as a potential wound healing agent via network pharmacology molecular docking and molecular dynamics simulation. Int J App Pharm. 2024;16(2):188-94. doi: 10.22159/ijap.2024v16i2.49922.